JAST, Vol. 7, No. 1, pp 1–8

JAST
Journal of Aerospace Science and Technology

The Multidisciplinary Design Optimization of a Reentry Vehicle Using Parallel Genetic Algorithms

S.A. Moosavi[1], M. Mirzaei[2] and J. Roshanian[3]

The purpose of this paper is to examine the multidisciplinary design optimization (MDO) of a reentry vehicle. In this paper, optimization of a RV based on minimization of heat flux integral and minimization of axial force coefficient integral and maximization of static margin integral along reentry trajectory is carried out. The classic optimization methods are not applicable here due to the complexity of the equations. Therefore, in this research, the genetic algorithm technique is utilized for optimization of the RV. In addition, the results of the genetic algorithm are validated with those of two other methods, Pareto genetic algorithm and response surface method. In the present paper, in order to decrease the computational time, parallel processing strategy is employed here.

INTRODUCTION

An RV experiences hypersonic and supersonic flight regimes during reentry to atmosphere. Therefore, it is an important problem to design an RV with minimum integrated drag during the entire flight mission while satisfying heat-transfer constraints. The aerodynamic design of an RV strongly influences the design of other subsystems (disciplines), *i.e.* structure, propulsion system, control, and thermal protection system. For instance, during the reentry to the atmosphere, an RV experiences high heat transfer rate due to aerodynamic heating phenomenon. Consequently, its structure is imposed to high gradient thermal stresses that may cause the failure of the structure. An optimized aerodynamic configuration can reduce the se the failur re imposed to thermal stress number flight condition, an RV experiences effects of thermal stresses on the structure.

1. *M.Sc. Student, Dept. of Aerospace Eng., K.N. Toosi Univ. of Tech., Tehran, Iran, Email: seyed.ali.moosavi5574@gmail.com.*
2. *Associate Professor, Dept. of Aerospace Eng., K.N. Toosi Univ. of Tech., Tehran, Iran, Email:Mirzaei@kntu.ac.ir.*
3. *Associate Professor, Dept. of Aerospace Eng., K.N. Toosi Univ. of Tech., Tehran, Iran, Email:roshanian@kntu.ac.ir.*

Optimization of an RV configuration based on an aerodynamic discipline may not necessarily lead to an optimized configuration and interactions of the aerodynamic discipline with other disciplines should be considered in configuration design and optimization. Moreover, optimization of a configuration only in a specified condition will not result in an optimized configuration for the whole the flying trajectory. Consequently, integrated design optimization based on the whole trajectory should be considered in configuration design and optimization.

Many papers have been published regarded on configuration design optimization with considering the aerodynamic discipline besides other disciplines. Monti *et.al.* worked on optimization of an RV configuration based on structure and aerothermodynamic disciplines for the point of maximum dynamic pressure. Gang *et.al.* designed optimized control and guidance subsystems for a specified configuration with considering the aerodynamic discipline. Jianjun *et.al.* linked geometry, aero/aero thermal, and trajectory together in a collaborative engineering environment to form a multidisciplinary analysis model of an RV performing atmospheric reentry.

In this research, integration of the aero thermodynamic heat flux and integration of the axial drag coefficient on an RV are intended to be minimized

during the entire reentry flight. This multi-disciplinary procedure have not been reported in similar works.

PROBLEM STATEMENT

The problem we are dealing with is minimization of the integration of the produced heat flux and the integration of the axial drag coefficient. The generay configuration of the RV vehicle is displayed in Figure 1, blunt nose radius and the angle of the conical parts are considered as design variables. Moreover, tangency of the first crank to the spherical nose is an inequality nonlinear constraint function. The lengths of conical and cylindrical parts (L1, L2, L3) are constant. It should be noted that due to the variation of the design variables, the total length as well as the base diameter of the RV may change.

Traditional search optimization approaches search from point to point and result in one optimal design. One common approach is the weighted objectives approach. In this approach, the objective function of the problem is expressed as $\hat{\phi}(x) = \alpha_1\phi_1(x)+\alpha_2\phi_2(x)+ ... + \alpha_{n_{obj}}\phi_{n_{obj}}(x)$.

NSGA-II algorithm is a good multi-objective genetic optimization algorithm based on Pareto-optimal approach. NSGA-II has good performance in design and can produce all of the optimal results for different weighting factors.

Parameters of the genetic algorithm and multi-objective Pareto genetic algorithm are presented in Table 1. Using these two methods, we generally reach the neighborhood of the minimum point. Fmincon and Fgoalattain hybrid functions are used in genetic and Pareto algorithms respectively to make sure that the minimum point is achieved. These hybrid functions which are gradient-based optimizers, are executed after finishing the genetic algorithm and Pareto genetic algorithm procedures. Furthermore, the number of the iterations is increased to avoid approaching a local minimum point. Mutation function, Mutation adapt feasible, randomly generates directions that are adaptive with respect to the last successful or unsuccessful generation. The feasible region is bounded by the constraints and inequality constraints. A step length is chosen along each direction so that linear constraints and bounds are satisfied.

In the present work, parallelization of the genetic algorithm means that, equal to the number of produced individuals (RV) in each generation, the flight simulation must be run and since running these simulations is independent of each other, hence these simulations can be run using parallel processing.

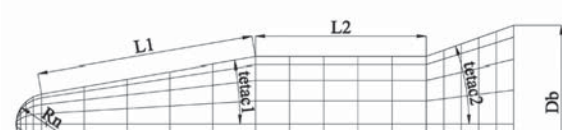

Figure 1. The design variables which Vary within a specific range.

It should be noted that, since the aerothermodynamic computations are carried out in each step in the flight simulation, the simulation takes nearly 15-20 minutes in a 3.4 GHZ processor. Therefore, the need to parallel genetic and Pareto algorithms may reduce the computational time considerablely. The computations were performed on a 16-3.4 GHZ cluster processor. The run time for parallel simulation was about 12.48 hours.

Response Surface Method (RSM) with second-order polynomials can reduce the number of iterations. The design space stretching technique through the design variable transformation can be used to represent the highly nonlinear behavior of the objective function and design constraints effectively.

Central composite designs (CCDs), is shown in Figure 2. One of the designs of the experiment theories is used to determine the experimental points needed to build the response surface. The response surface method is an n-factor, second-order design, where a minimum number of experimental points are used to minimize the variance by maximizing the determinant of $\left|X^T X\right|$.

Where X is the design matrix, fifty experimental points are finally selected. This is the recommended number of points required to build relatively accurate regression models. The following equation represents the generic form of the second-order response surface equation used in this study:

$$R = b_0 + \sum_{i=1}^{k} b_i x_i + \sum_{i=1}^{k} b_{ii} x_i^2 + \sum_{i=1}^{k-1} \sum_{j-i+1}^{k} b_{ij} x_i x_j \qquad (1)$$

where R is the response (heat flux integral and axial force coefficient integral in this study), b_0 is the constant coefficient, b_i is the regression coefficient for

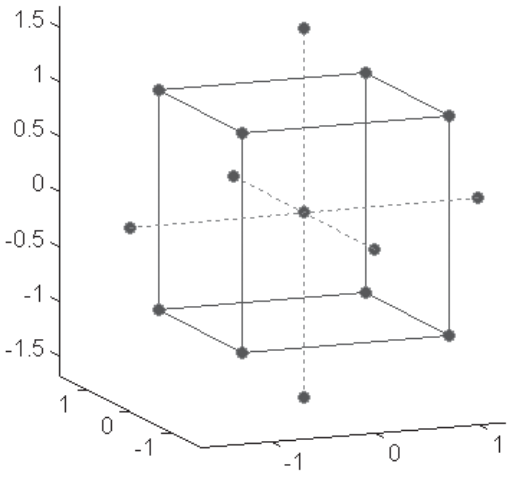

Figure 2. Central composed design-circumscribed.

Table 1. Pareto Genetic Algorithm and Genetic Algorithm parameters.

B) Pareto Genetic Algorithm		A) Genetic Algorithm	
45	Generations	45	Generations
24	Population Size	24	Population Size
5*pi/180(rad) 10*pi/180(rad) 0.15(m)	Lower Bound	5*pi/180(rad) 10*pi/180(rad) 0.15(m)	Lower Bound
10*pi/180(rad) 15*pi/180(rad) 0.3(m)	Upper Bound	10*pi/180(rad) 15*pi/180(rad) 0.3(m)	Upper Bound
Mutation adapt feasible	Mutation Function	Mutation adapt feasible	Mutation Function
F(1) = 10e6*Sum(Cx(:)) F(2) = Sum(flux(:)) F(3) = 10e6*(1/Sum(abs(st(:))))	Fitness Function	0.2*10e6*Sum(Cx(:)) +0.7*Sum(flux(:)) +0.1*10e6*(1/Sum(abs(st(:))))	Fitness Function
fgoalattain	Hybrid Function	Fmincon	Hybrid Function

the first-order terms, b_{ii} is the coefficient for the pure quadratic terms, b_{ij} is the coefficient for the cross-product terms, $x_{i,j}$ is the design variable (shape function parameters), and k is the number of design variables.

REENTRY TRAJECTORY MODEL

The vehicle trajectory is calculated by a three-dimensional point mass model for the vehicle of constant mass flying over a spherical planet with a stationary atmosphere. The 6 DOF re-entry flight dynamics and kinetics was modeled, In order to achieve the minimum restriction and singularities, quaternion representation of vehicle attitude was used to avoid computational singularities in the angular kinetic equations. These equations are given in this section. The earth atmosphere was modeled based on the 1962 Standard Atmosphere Model and the Global Reference Atmospheric Model of 99. Flight initials conditions are presented in Table 2. Some of the results of the 6DOF simulation for the optimum shape obtained by genetic algorithm are presented in Figure 3.

Table 2. Flight initial conditions.

4300(m/s)	v
-15deg	θ
15deg	ν
30deg	α
82km	Height
0(rad/s)	p,q,r

Table 3. Engineering methods

	inviscid flow	viscous flow
1	Blunt body	Reference Enthalpy
2	Modified Newtonian	Spalding - chi
3	Modified Newtonian plus prandtl meyer	
4	Tangent cone	
5	High mach number	

AEROTHERMODYNAMIC CALCULATIONS

Aerodynamic and aerothermodynamic calculations are performed using semi-empirical relations. Table 3 presents some of the methods employed in the current study. In this table, the methods are categorized into inviscid and viscous groups. For calculation of the aerodynamic coefficients resulting from pressure for flows with Mach less than or equal to 5, the engineering methods 2 and 4; for impact regions, methods 2 and 3; and for shadow regions, method 5 are used. For flows with Mach number more than 5, the engineering methods 1 and 2; for impact regions, and for shadow region, the engineering methods 2 and 5 s are used. For regions where the flow separation occurs, the viscous flow model is employed.

In the following, we present more details about the methods given in Table 3 .

Inviscid Pressure Methods

Blunt Body Empirical Ohio State University (OSU)
The experimental information obtained for a cylinder shows that the surface pressure to free stream static pressure ratio is independent of Mach number and Reynolds number. The experimental method for blunt bodies gives an empirical relation for the pressure ratio-curvature angle as follows:

$$\frac{p}{p_\infty} = 0.32 + 0.455\cos\theta + 0.195\cos 2\theta + 0.035\cos 3\theta - 0.005\cos 4\theta \quad (2)$$

The above relation formulates the information obtained for a cylinder and has a maximum error of 2.5%. Even when our models involve attack angle, the results have very good agreement.

In the above equation, θ is the circumference angle of the cylinder which is zero at the Stagnation point, and p_1 and p_{0_∞} are surface pressure and Stagnation pressure behind the impact wave respectively.

The pressure coefficient is obtained as:

$$c_p = \left[\left(\frac{p_1}{p_{0_\infty}}\right)\left(\frac{p_{0_\infty}}{p_\infty}\right) - 1 \right] / \frac{\gamma}{2} M^2 \quad (3)$$

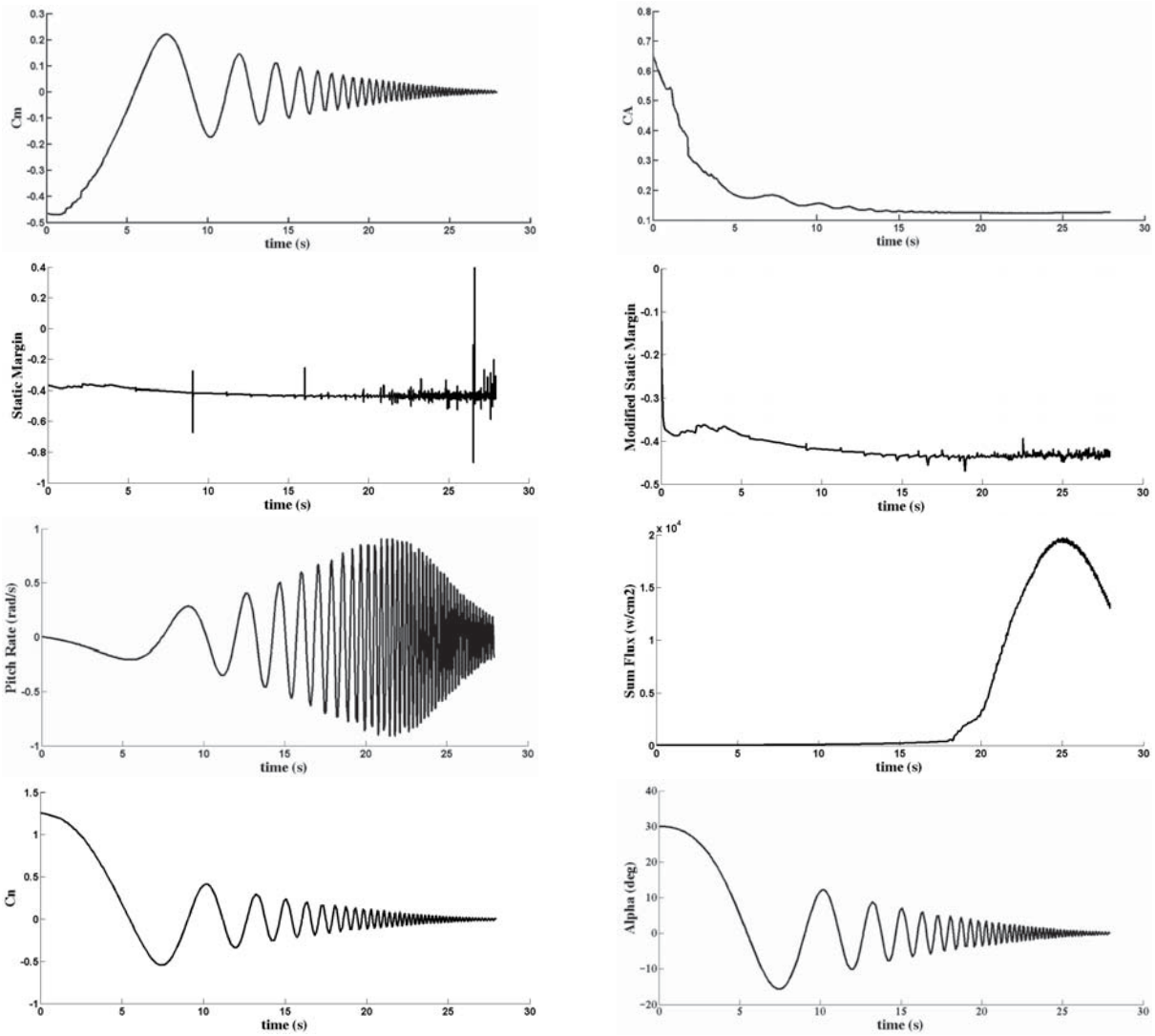

Figure 3. Results of simulation.

$$\frac{p_{0\infty}}{p_\infty} = k\frac{\gamma}{2}M^2 + 1 \tag{4}$$

Modified Newtonian Plus Prandtl Meyer

This method, described as the blunt body Newtonian plus Prandtl Meyer technique, is based on the analysis presented by Kaufman in Reference 21. The flow model used in this method assumes a blunt body with a detached shock followed by an expansion around the body to supersonic conditions. This method uses a combination of the modified Newtonian and Prandtl Meyer expansion the theory. Modified Newtonian theory is used along the body until a point is reached where both the pressure and the pressure gradients match those that would be calculated by a continuing Prandtl Meyer expansion.

The calculation procedure derived for determining the pressure coefficient using the blunt body Newtonian plus Prandtl Meyer technique is outlined below:

1. Calculate free stream static to stagnation pressure ratio.

$$P = \frac{P_\infty}{P_0} = \left[\frac{2}{(\delta+1)M_\infty^2}\right]^{\frac{\delta}{\delta-1}} \left[\frac{2\delta M_\infty^2 - (\delta-1)}{\delta+1}\right]^{\frac{1}{\delta-1}} \tag{5}$$

2. Assume a starting value of the matching Mach number, M_q (for $\delta = 1.4$ assume $M_q = 1.35$).
3. Calculate the matching point to free stream static pressure ratio.

$$Q = \frac{P_q}{P_0} = \left[\frac{2}{2+(\delta-1)M_q^2}\right]^{\frac{\delta}{\delta-1}} \tag{6}$$

4. Calculate the new free stream static to stagnation pressure ratio.

$$P_C = Q\left[1 - \frac{\delta^2 M_q^4 Q}{4(M_q^2 - 1)(1 - Q)}\right]^{\frac{\delta}{\delta - 1}} \tag{7}$$

5. Assume a new matching point Mach number (1.75) and repeat the above steps to obtain a second set of data.
6. With the above two tries, use a linear interpolation equation to estimate a new matching point Mach number. This process is repeated until the solution converges.
7. Calculate the surface slope at the matching point.

$$\sin^2 \delta_q = \frac{Q - P}{1 - P} \tag{8}$$

8. Use the Prandtl Meyer expansion equations to find the Mach number on the surface element, M_δ.
9. Calculate the surface pressure ratio.

$$Q = \frac{P_\delta}{P_0} = \eta_C \left[1 + \frac{\delta - 1}{2} M_\delta^2\right]^{-\frac{\delta}{\delta - 1}} \tag{9}$$

Where η_C is provided as an empirical correction factor and P_δ is the pressure on the element of interest.

10. Calculate the surface to free stream pressure ratio.

$$\frac{P_\delta}{P_\infty} = (\frac{1}{P})(\frac{P_\delta}{P_0}) \tag{10}$$

11. Calculate the surface pressure coefficient.

$$C_{P_\delta} = \left[\frac{2}{\gamma M_\infty^2}\right](\frac{P_\delta}{P_\infty} - 1) \tag{11}$$

As pointed out in several references, this correlation has good agreement with the experimental data for blunt shapes. However, if the surface curvature changes gradually to zero slopes, at some distance from the blunt stagnation point, the pressure calculated by this method will be too high. This is caused by the characteristics near the nose intersecting the curved shock system and being reflected back onto the body.

High Mach Number

For a reentry vehicle at a high velocity, the back areas are expected to be in vacuum, *i.e.*:

$$c_p = -\frac{1}{\frac{\gamma}{2} M_\infty^2} \tag{12}$$

At the back areas, there is a little pressure due to the viscosity of the gas. The experimental information shows that this vacuum is approximately 70% in the air, so the expression of the pressure coefficient will be:

$$c_p = -\frac{1}{M_\infty^2} \tag{13}$$

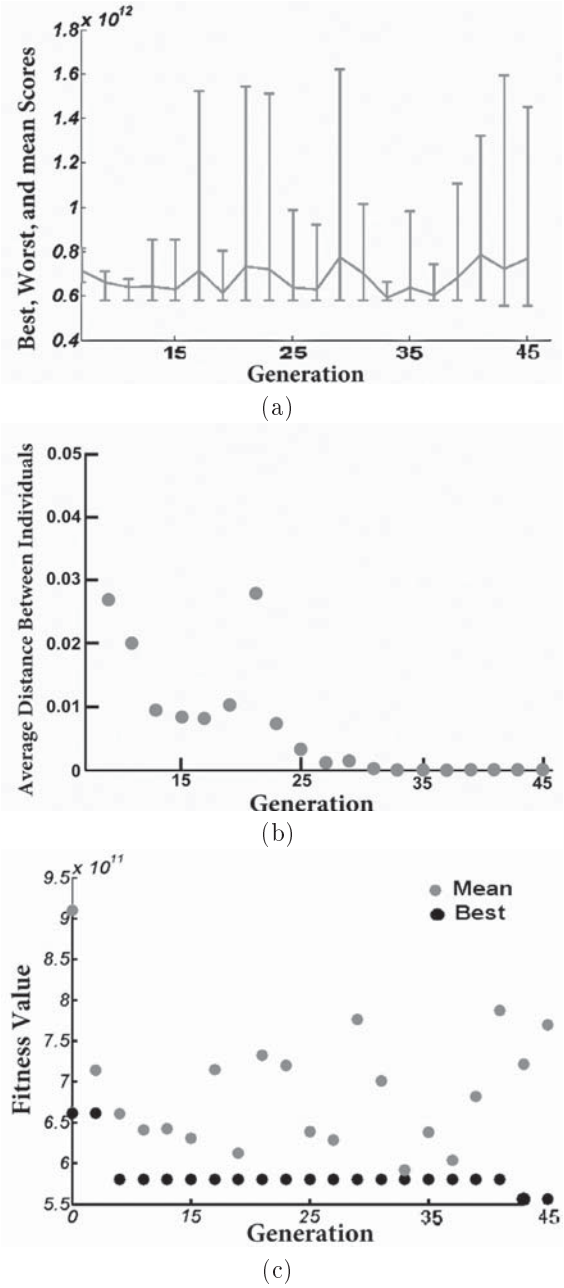

Figure 4. (a) A vertical line at each generation, showing the range from the smallest to the largest fitness value, as well as mean fitness value, (b) The average distance between individuals in each generation, (c) Best and Mean Fitness Value in each generation.

Viscous Force Calculation Methods

In this part, two methods are presented to estimate the surface friction and heat transfer in hypersonic laminar and turbulent flows. One of these methods, the base thermal degree method, is similarly used for the both laminar and turbulent flows while the second method is merely applicable for turbulent flows.

Table 4. Validation with CFD solver – Ca.

Mach	Alpha(deg)	Height(km)	CFD	Subroutine	Diff%
4	0	10	0.28949	0.3117	7.6
4	10	10	0.318	0.32748	2.98
5	0	10	0.2497754	0.28289	13.25
5	10	10	0.2797982	0.30089	7.53
10	0	8	0.1909151	0.16061	-15.87
10	10	8	0.2258	0.17076	-24.37
14	0	60	0.2102048	0.18151	-13.65
14	10	60	0.2498	0.19207	-23.11

Table 5. Validation with CFD solver - Cn.

Mach	Alpha(deg)	Height(km)	CFD	Subroutine	Diff%
4	0	10	0	0	0
4	10	10	0.352	0.4052	15.11
5	0	10	0	0	0
5	10	10	0.3248	0.3937	21.21
10	0	8	0	0	0
10	10	8	0.2708	0.2856	5.46
14	0	60	0	0	0
14	10	60	0.249	0.287	15.26

Spalding Chi Method

The local skin friction coefficient over a flat plate for hypersonic flow depends on γ, Re_x, M_e and T_w/T_e (hypersonic similarity parameters), that is:

$$c_f = c_f(\mathrm{Re}_x, M_e, T_w/T_e, \gamma) \tag{14}$$

Spalding and Chi presented a method based on the assumption of a unique relation between $c_f F_c$ and $\mathrm{Re}_x F_{Re}$, where F_c and F_{Re} are coupling parameters which dependent on temperature to Mach number ratio.

The values of F_c and F_{Re} for air ($\gamma = 1.4$) are presented in references 14 and 15.

Having the flow conditions and the surface temperature, and also having F_c, F_{Re}, $c_f F_c$, and $\mathrm{Re}_x F_{Re} c_f$ can be determined.

The method 1 is employed for calculations of aerodynamic coefficients due to friction as well as thermal flux in laminar viscous flows and the method 2 is used for calculation of turbulent viscous flows.

RESULTS

To validate the semi-empirical calculations, the results are compared with those of CFD calculations. This comparison is presented in Tables 4 to 6. In these tables, the aerodynamic coefficients of the RV from the semi-empirical and the CFD methods are compared. Table 4 gives axial force coefficients at various flight conditions. It can be seen that the maximum deviation of the semi-empirical results from those of CFD is 23% . This deviation in a normal force coefficient (CN) is 21% (Table 5) and in a pitching moment coefficient (CM) is 16% (Table 6). These deviations show that the semi-empirical calculations can be used as a proper tool in design and optimization calculations.

In Figure 4, the curves resulting from the execution of scalar genetic algorithm with specifications given in Table 1A are shown. Figure 4a shows a vertical line in each generation whose its upper, lower and middle limits respectively show the measure and the prominence related to the maximum, the minimum and the average of the objective function at the relevant generation.

As it is seen, the more the upper and the lower limits of the line approach each other, it implies the a less jump occurs in the respective generation. Figure 4b shows the average distance between the points, *i.e.* chromosomes, in each generation. In this figure, too, the more the average distance between the chromosomes approaches to zero, the less jump occurs in that generation. Figure 4c illustrates the average and the minimum values of the objective function in each generation. As it is seen, the more we approach the end of the genetic algorithm execution, the more reduction occurs in the distance between the average and the minimum values of the objective function extremely reduces.

Pareto genetic algorithm, as its name shows, gives some results which none of them has any special advantages over the others and the designer should decide on choosing the proper configuration. In other words, executing the pareto genetic algorithm is equivalent to executing the scalar genetic algorithm for different weights of the objective function. Figures 5 show the curves resulted from executing pareto genetic algorithm with specifications given in Table 1B. In Figure 5a, the three dimensional form of the pareto front for vectorial objective function with three components is shown. Figure 5b, Figure 5c and Figure 15d illustrate the variation of the vectorial objective function components in double forms. In Figures 5, it is seen that the scalar genetic algorithm result has been located in pareto front of the pareto genetic algorithm. So, pareto genetic algorithm confirms the results obtained by scalar genetic algorithm. In Table 7, in addition to the results for the respective objective functions in vectorial and scalar genetic algorithms, the optimum

Table 6. Validation with CFD solver - Cm

Mach	Alpha(deg)	Height(km)	CFD	Subroutine	Diff%
4	0	10	0	0	0
4	10	10	0.542	0.60396	11.43
5	0	10	0	0	0
5	10	10	0.5045	0.58749	16.44
10	0	8	0	0	0
10	10	8	0.424	0.43831	3.375
14	0	60	0	0	0
14	10	60	0.374	0.43456	16.19

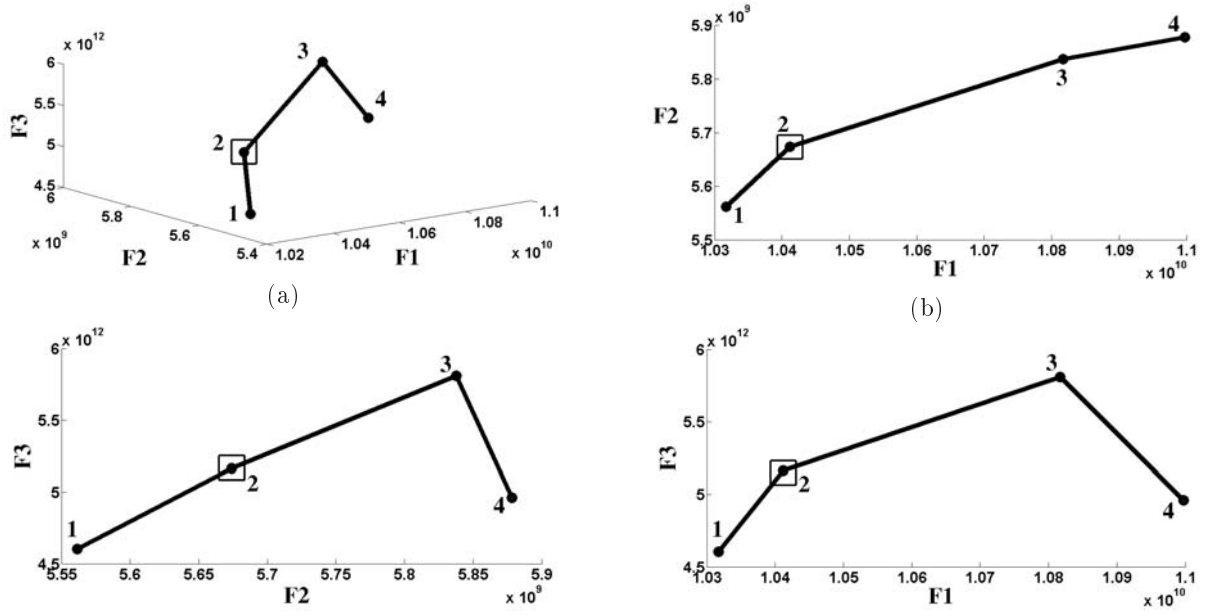

Figure 5. (a) The three dimensional form of the pareto front, (b) The variation of the vectorial objective function components in double forms, (c) The variation of the vectorial objective function components in double forms, (d) The variation of the vectorial objective function components in double forms.

configurations resulted from both algorithms based on the design variables are also presented.

In RSM method, similar to the scalar genetic algorithm method, the objective function has been considered in nonvectorial form. As it is seen in Figure 6, firstly, the objective function values for 17 predictor points are obtained in an offline manner from the flight simulation. Secondly in the specified domain of the design variables, the objective function is calculated by RSM for the whole design space. Table 8 shows the difference between the optimum configurations resulted from scalar genetic algorithm and RSM. It is seen that there is a little difference between the results of the two methods. Since RSM does not calculate the objective functions in an online manner, but rather it guesses the objective function values, the objective function value obtained for the configuration resulted from RSM should be compared with its real value resulted from flight simulation for the same configuration. This comparison has been done in Table 9 in which a little difference is seen between the objective function value calculated by RSM and its real value.

Table 8. Difference Between Results of GA and RSM.

Variable	thetac1 (rad)	thetac2 (rad)	Rn (m)
GA	0.155727	0.191795	0.20638
RSM	0.1596	0.1879 0.2085	
Diff%	2.5003	2.0337	1.0075

Table 9. Difference Between Calculated Fitness Value and Real Fitness Value.

Calculated Value	522566321068.260
Real Value	565385440921.823
Diff%	7.5734

CONCLUSIONS

In this paper, optimization of an RV based on minimization of heat flux integral and minimization of axial force coefficient integral along reentry trajectory was carried out. Semi empirical methods were used for aerodynamic and aero heating calculations. A comparison of the results of the methods with those of

Table 7. Results of Pareto Genetic Algorithm and Genetic Algorithm.

Point	F1	F2	F3	thetac1(rad)	thetac2(rad)	Rn(m)
1	46031518318824.87	5561613281.09753	10317123753.6537	0.2140	0.2292	0.1382
2(GA)	5165120394485.97	5674185057.20986	10411760398.0818	0.2064	0.1918	0.1557
3	5809687701099.58	5837682372.12098	10816653212.4112	0.2150	0.1876	0.1314
4	4962295734064.01	5878443378.83571	10997703260.1690	0.2070	0.2223	0.1528

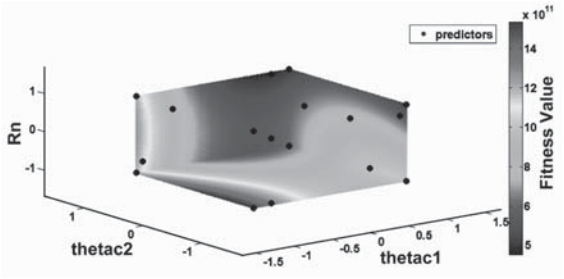

Figure 6. Change of the objective function in model response.

the CFD shows that these methods were proper tools for these calculations. The RSM optimization method predicted a lot of local minimum points that cannot be captured with gradient- based optimization methods. However, search- based methods (algorithm and genetic Pareto genetic algorithm) can find the absolute minimum point and the results of RMS validate the results of these two search methods.

REFERENCES

1. Monti R., Fumo M.D.S., and Savino R., "Thermal Shielding of a Reentry Vehicle by Ultra-High-Temperature Ceramic Materials", *AIAA Journal*, **20**(3), (2006).
2. Gang C., Min X., Zi-ming W., and Si-lu C., "RLV Reentry Trajectory Multi-objective Optimization Design Based on NSGA-II Algorithm", *AIAA Paper 2005-613, Presented at the AIAA Atmospheric Flight Mechanics Conference*, (2005).
3. Jianjun L., Wenyong Z., Qun F., and Jianping Y., "An Integrated Optimization of RLV Reentry Trajectory", *IAC-03-A.7.05, Presented at the 54th International Astronautical Congress of the International Astronautical Federation*, (2003).
4. Kalyanmoy D., *Multi Objective Optimization Using Evolutionary Algorithms*, John Wiley & Sons, (2001).
5. Anderson M.B., and Lawrence W.R., "Launch Conditions and Aerodynamic Data Extraction by an Elitist Pareto Genetic Algorithm", *AIAA Paper 96-3361, Presented at the AIAA Atmospheric Flight Mechanics Conference*, (1996).
6. Conn A.R., Gould N.I.M. and Toint Ph.L., "A Globally Convergent Augmented Lagrangian Barrier Algorithm for Optimization with General Inequality Constarints and Simple Bounds", *Mathematics of Computation*, **66**(217), PP 261-288(1997).
7. Walts R.A., "An Interior Algorithm for Nonlinear Optimization that Combines Line Search and Trust Region Steps", *Mathematical Programming*, **107**(3), PP 391-408(2006).
8. Powell M.J.D., "A Fast Algorithm for Nonlinear Constrained Optimization Calculaitons", *Numerical Analysis, Lecture Notes in Mathematics*, **630**, (1978).
9. Kepner J., Ahalt S., "MatlabMPI", *Journal of Parallel and Distributed Computing*, **64**, PP 997-1005(2004).
10. The Mathworks, Inc., "Distributed Computing Toolbox 3.1 User's Guide", .
11. Lee J.W., Min B.Y., and Byun Y.H., "Multipoint Nose Shape Optimization of Space Launcher Using Response Surface Method", *JOURNAL OF SPACECRAFT AND ROCKETS*, **43**(1), (2006).
12. Costa R.R., Silva S.F.W., Chu Q.P. and Mulder J.A., "Atmospheric Re-entry Modeling and Simulation: Application to a Lifting Body Re-Entry Vehicle", *AIAA Paper 2000-4086, Presented at the AIAA Modeling and Simulation Technologies Conference*, (2000).
13. Gu D.W., Petkov P.H. and Konstantinov M.M., *Robust Control Design with MATLAB*, (2005).
14. Guidi A., Chu Q.P., Mulder J.A., Nicolosi F., "Virtual Reality Modeling Simulation of the Re-Entry Motion of an Axialsymmetric Vehicle", *AIAA Paper 2002-4968, Presented at the AIAA Modeling and Simulation Technologies Conference*, (2002).
15. Bertin J.J. and Smith M.L., *Aerodynamics for Engineers*, Prentice-Hall International Edition, (1989).
16. Anderson J.D., *Hypersonic and High Temperature Gas Dynamics*, Mc.Graw - Hill Book Co., (1989).
17. Panagiotopoulos E.E., Margaris D.P. and Papanikas D.G., "Aero Thermodynamic Analysis and Real Gas Flow Properties of Spacecraft Hypersonic Entry Flight", *AIAA Paper 2006-3250, Presented at the 9th AIAA/ASME Joint Thermophysics and Heat Transfer Conference*, San Francisco, CA, (2006).
18. Arvel E.G., Douglas N.S. and Wayne R.O., "The MARK IV Supersonic-Hypersonic Arbitrary-Body Program", *Program Formulation Volume II, Douglas Aircraft Company Mcdonnell Douglas Corporation*, (1979).
19. Zoby E.V., Moss J.N. and Sutton K., "Approximate Convective-Heating Equations for Hypersonic Flows", *Journal of Space Craft and Rockets*, **18**(1), PP 64-70(1981).
20. Eckerts E.R.G., "Engineering Relations for Heat Transfer and Friction in High Velocity Laminar and Turbulent Boundary Layer Flow Over Surfaces with Constant Pressure and Temperature", *Trans. of the ASME*, **78**(6), (1956).
21. Bertin J.J. and Smith M.L., *Aerodynamics for Engineers*, Prentice - Hall International Editions, (1989).
22. Spalding D.B. and Chi S.W., "This Drag of a Compressible Turbulent Layer on a Smooth Flat Plate with and without Heat Transfer", *Journal of Fluid Mechanics*, **19**, PP 117-143(1964).